AGU PUBLICATIONS

Geophysical Research Letters

RESEARCH LETTER
10.1002/2016GL069650

Key Points:
- We present an SV tomographic model of the Earth's mantle that includes new normal mode observations
- Near the CMB, we observe an odd/even degree amplitude ratio larger than in previous models
- Near the CMB, the broad-scale velocity pattern is more complex than expected from a dominant degree 2

Supporting Information:
- Supporting Information S1

Correspondence to:
S. Durand,
durand@uni-muenster.de

Citation:
Durand, S., E. Debayle, Y. Ricard, and S. Lambotte (2016), Seismic evidence for a change in the large-scale tomographic pattern across the D'' layer, *Geophys. Res. Lett.*, *43*, 7928–7936, doi:10.1002/2016GL069650.

Received 18 MAY 2016
Accepted 19 JUL 2016
Accepted article online 23 JUL 2016
Published online 4 AUG 2016

Seismic evidence for a change in the large-scale tomographic pattern across the D'' layer

S. Durand[1,2], E. Debayle[1], Y. Ricard[1], and S. Lambotte[3]

[1] Laboratoire de Géologie de Lyon-Terre, Planètes, Environnement, CNRS, UMR 5276, École Normale Supérieure de Lyon, Université de Lyon, Université Claude Bernard Lyon 1, Villeurbanne, France, [2] Institut für Geophysik, Münster, Germany, [3] Institut de Physique du Globe de Strasbourg, UMR 7516, Université de Strasbourg, EOST/CNRS, Strasbourg, France

Abstract We present SEISGLOB1, a pure SV tomographic model of Earth's mantle based on Rayleigh phase velocities and normal mode self- and cross-coupling data. SEISGLOB1 is the first model that incorporates the cross-coupling of normal modes since the pioneering work of Resovsky and Ritzwoller (1999). The simultaneous inversion of new cross-coupling normal modes and self-coupling of high-order normal modes measured by Deuss et al. (2013) and Stoneley modes measured by Koelemeijer et al. (2013) allows us to show that the velocity structure at the base of the mantle is more complex than that expected from a dominant spherical harmonic degree 2 and that the relative strength of odd degrees has previously been underestimated. Near the core-mantle boundary, the large low-shear-velocity provinces are less homogeneous than in previous studies, and various local maxima, often potentially associated with hot spot sources, are observed.

1. Introduction

The lowermost few hundred kilometers of Earth's mantle corresponds to the D'' region [*Bullen*, 1949]. This region above the core-mantle boundary (CMB) marks the transition between the molten iron alloy of the outer core and the solid silicates of the lower mantle across which heat and possibly some material are exchanged. This layer thus plays a critical role not only in mantle convection but also in core convection, Earth's heat budget and geodynamo process. Therefore, any change in the lower mantle large-scale structure would have great implications in our understanding of the outer core dynamics [*Amit et al.*, 2008; *Bloxham*, 2000; *Olson et al.*, 2010; *Gubbins et al.*, 2011; *Driscoll*, 2015]. Seismology has revealed that the D'' region is dominated by a degree 2 pattern of low-velocity heterogeneities [*Dziewonski et al.*, 1977], with maximum amplitudes beneath Pacific and Africa, surrounded by a high-velocity circum-Pacific rim commonly interpreted as the imprint of Mesozoic subduction slabs [*Ricard et al.*, 1993].

The structure of the lowermost mantle has been constrained until today by both body waves and normal modes self-coupling [*Ritsema et al.*, 2011; *Moulik and Ekström*, 2014; *French and Romanowicz*, 2015; *Koelemeijer et al.*, 2016]. However, these data have two main disadvantages. First, the self-coupling of normal modes used to constrain the previous 3-D models is only sensitive to the even spherical harmonic degrees of the mantle structure. Second, even though both even and odd spherical harmonic degrees can in principle be constrained by body waves, their limited coverage due to the uneven distribution of earthquakes and seismic stations may oversample the degree 2 at the base of the mantle.

In this paper, we present SEISGLOB1, an *S* wave model of the Earth's mantle constrained by a data set of Rayleigh wave phase velocities and of normal mode self- and cross-coupling coefficients, including Stoneley modes. SEISGLOB1 is the first model that incorporates the cross-coupling of normal modes in the inversion since *Resovsky and Ritzwoller* [1999], 17 years ago. The simultaneous inversion of new normal mode cross-coupling and high-order self-coupling data [*Deuss et al.*, 2013], and Stoneley mode self-coupling data [*Koelemeijer et al.*, 2013] allows us to provide constraints on both even and odd spherical harmonic degrees, thus refining our view of the broad-scale seismic structure (up to degree 8) near the bottom of the mantle. We first present the data and the inversion method that have been used to build SEISGLOB1. We then show that SEISGLOB1 exhibits a new pattern of large-scale shear wave heterogeneities at the base of the mantle. Finally, we discuss the implications of this pattern for outer core dynamics.

2. Data and Inversion Method

SEISGLOB1 is based on a global data set of Rayleigh phase velocity measurements [*Durand et al.*, 2015], completed by a global compilation of the currently available self-coupling [*Smith and Masters*, 1989; *Resovsky and Ritzwoller*, 1998; *Masters et al.*, 2000; *Deuss et al.*, 2013; *Koelemeijer et al.*, 2013] and cross-coupling [*Resovsky and Ritzwoller*, 1998; *Deuss et al.*, 2013] coefficients of spheroidal normal modes. We include higher radial order modes (up to the branch 19) and Stoneley modes, thanks to the recent catalogs published by *Deuss et al.* [2013] and *Koelemeijer et al.* [2013] (see Table S1 in the supporting information). We also include cross-coupling normal mode data (see Table S2 in the supporting information), which were not incorporated in recent tomographic models. Normal mode cross-coupling is induced by 3-D heterogeneities in the Earth but has the advantage, compared to the self-coupling of normal modes, to be sensitive to either even or odd spherical harmonic degrees. Until recently, the number of published cross-coupling structure coefficients was limited. In 1998, *Resovsky and Ritzwoller* [1998] published cross-coupling structure coefficients for nine pairs of modes only, but this has been recently extended by *Deuss et al.* [2013] up to 32 pairs of modes.

Body wave travel times have been excluded from the inversion on purpose, because body wave travel times are generally measured on transverse components and thus are sensitive to the velocity of horizontally polarized seismic waves (SH waves), while our current data set (Rayleigh waves and spheroidal modes) is sensitive to vertically polarized seismic waves (SV waves). Radial anisotropy, which is known to be locally strong at the bottom of the mantle [*Kendall and Silver*, 1996; *Ritsema*, 2000; *Ford et al.*, 2006], leads to differences in the velocities of SH and SV waves. If not properly accounted for, radial anisotropy variations can trade off with the large-scale isotropic structure [*Chang et al.*, 2015]. For this reason, we choose to build a pure SV model by excluding body waves. In addition, this enables us to overcome the uneven body wave coverage at the base of the mantle. Moreover, since we are only interested in the large-scale structure at the base of the mantle, the exclusion of body wave data should not affect the results of our study.

The Rayleigh surface wave data set established by *Durand et al.* [2015] includes some 22,000,000 Rayleigh wave phase velocity measurements with their associated errors. These measurements have been obtained applying an automated waveform inversion approach [*Debayle and Ricard*, 2012] on some 534,359 seismograms, in the period range 40–360 s for the fundamental mode and up to the fifth overtone. From these measurements, done on individual seismograms, a smooth phase velocity map is produced at each period applying a continuous regionalization [*Tarantola and Valette*, 1982; *Montagner*, 1986; *Debayle and Sambridge*, 2004]. The phase velocity maps are then decomposed into spherical harmonics up to the degree 20, and the spherical harmonic coefficients, denoted σ_s^t, constitute the first part of the inverted data. Their associated errors are computed from the error maps provided by *Durand et al.* [2015]. This Rayleigh data set for the fundamental modes and its overtones, provides by itself a significant resolution of the mantle heterogeneities down to about 1000 km depth [*Durand et al.*, 2015].

In order to complete the sensitivity down to the lower mantle we also use spheroidal normal mode data. This data set contains splitting functions, $f(\theta, \phi)$, that represent the local perturbations of the center frequency of a normal mode due to the presence of aspherical heterogeneities into the Earth. The splitting function is expressed in terms of spherical harmonic expansion where the spherical harmonic coefficients, c_s^t, represent the so-called either self- or cross-coupling structure coefficients. We truncate the spherical harmonic expansion at degree 8, because we consider that above this degree the quality and the redundancy of the measurements is insufficient. In this study we use the measurements done by *Smith and Masters* [1989], *Masters et al.* [2000], *Resovsky and Ritzwoller* [1998], *Deuss et al.* [2013], and *Koelemeijer et al.* [2013]. We exclude the modes that are sensitive to the inner core since they display an anomalous self-coupling due to the inner core anisotropy [*Woodhouse et al.*, 1986]. In total, the normal mode data set contains 9214 self-coupling coefficients and 643 cross-coupling coefficients. Although the number of cross-coupling coefficient is limited, they provide new independent information on odd degrees, which are not constrained by self-coupling coefficients. Each measurement is provided with an estimated error which is used in the inversion.

Both phase velocity spherical harmonic coefficients, σ_s^t, and normal mode structure coefficients, c_s^t, are linearly related to the 3-D perturbations in P velocity, $(\delta\alpha/\alpha)_{st}$, S velocity, $(\delta\beta/\beta)_{st}$, density, $(\delta\rho/\rho)_{st}$, and topographies of discontinuities i, δh^i_{st}, by

$$c_s^t = \frac{U\omega}{c^2}\sigma_s^t = \int_0^a \left\{ \left(\frac{\delta\alpha}{\alpha}(r)\right)_{st} K_\alpha^s(r) + \left(\frac{\delta\beta}{\beta}(r)\right)_{st} K_\beta^s(r) + \left(\frac{\delta\rho}{\rho}(r)\right)_{st} K_\rho^s(r) \right\} dr + \sum_i \delta h^i_{st} K_i^s \quad (1)$$

where K_α^s, K_β^s, K_ρ^s, and K_i^s are, respectively, the P velocity, S velocity, density, and interface topography sensitivity kernels at degree s [*Woodhouse*, 1980] computed in a 1-D reference model and c, U, and ω are, respectively, the phase velocity, group velocity, and angular frequency of the considered mode. The 1-D reference model is chosen to be PREM [*Dziewonski and Anderson*, 1981]. We invert for the mantle structure from the surface down to the CMB, so that no crustal corrections are performed. In order to reduce the computing time and because of a lack of resolution, we choose to neglect the interface topography effects, a reduction usually done in tomographic inversions [*Ishii and Tromp*, 2001]. In this study we present the results obtained assuming constant factors between P, S, and density perturbations, such that $\delta \ln(\alpha) = \nu_\alpha \delta \ln(\beta)$ and $\delta \ln(\rho) = \nu_\rho \delta \ln(\beta)$, where $\nu_\alpha = 0.55$ and $\nu_\rho = 0.2$ [*Ishii and Tromp*, 2001]. However, we also tested more complex depth-dependent (α, β) scalings that have been used in other recent tomographic models [*Ritsema et al.*, 2011; *Koelemeijer et al.*, 2016]. The results using these various scaling laws are discussed in the following sections; they support the results obtained with depth-independent scalings.

3. A New Large-Scale Pattern at the CMB

Figure 1 compares at 2700 and 2800 km depths SEISGLOB1 to three recent tomographic models (SEMUCB-WM1 [*French and Romanowicz*, 2014], S362WMANI+M [*Moulik and Ekström*, 2014], and SP12RTS [*Koelemeijer et al.*, 2016]) filtered out for degrees greater than eight in order to emphasize the new constraints obtained on the large-scale structure. The specificities of each model are summarized in Table S3. A comparison of SEISGLOB1 with the unfiltered other seismic models is provided in Figure S1 in the supporting information. SEMUCB-WM1 and S362WMANI+M are both 3-D radially anisotropic *S* wave models of Earth's mantle. SEMUCB-WM1 is based on the inversion of surface wave and body wave three-component waveforms, while S362WMANI+M is based on long-period body wave waveforms, short-period body wave travel times, surface wave phase velocities and normal mode self-coupling data. On the other hand, SP12RTS is a 3-D isotropic seismic model of Earth's mantle based on Rayleigh waves, body waves, and spheroidal modes. Like SEISGLOB1, SP12RTS includes self-coupling of high-order normal modes published by *Deuss et al.* [2013] and Stoneley observations published by *Koelemeijer et al.* [2013]. Unlike SEISGLOB1, SP12RTS does not account for the cross-coupling of normal modes in the inversion. SP12RTS is isotropic although it mixes SV waves (spheroidal modes, SKS waves) and SH waves (body waves except SKS). SEISGLOB1 is thus the only model that accounts for normal mode cross-coupling in the inversion.

Figure 1 shows that the two well-known large low-shear-velocity provinces (LLSVPs) under Pacific and Africa are present in all models. At 2700 km all models display very similar patterns of heterogeneities, and SEISGLOB1 is particularly similar to SEMUCB-WM1. SP12RTS displays weaker amplitudes than the three other models. At deeper depths, the pattern of anomalies changes significantly between SEISGLOB1 and the other models. The shape of the broad-scale low-velocity anomalies is more complex in SEISGLOB1 than that expected from a dominant degree 2. The LLSVP under Africa, mapped by the previous models as a rather homogeneous structure, appears much more patchy in SEISGLOB1 and is divided into four or five individual anomalies. The slowest zones near the CMB are found below the central Pacific, the mid and southern Atlantic, and the Nazca plate, and also under various hot spots or clusters of hot spots: for example, the Kerguelen-Crozet-Marion in the South Indian ocean or the Bouvet-Meteor in the South Atlantic ocean, the Afar or the Tasmanid hot spots. As a matter of fact, the only two slow zones of the CMB that do not seem related to the presence of hot spots are north of the Caspian sea and in the northern part of the Pacific. These two slow patches are also found in the other models and the former has been sometimes named the Perm anomaly [*Lekic et al.*, 2012]. The low-velocity anomaly beneath the Afar, distinct from the African LLSVP, is much more conspicuous than in the other tomographic models. Until now, the source of the Afar hot spot has been either located in the midmantle [*Debayle et al.*, 2001; *Benoit et al.*, 2006; *Chang and Van der Lee*, 2011] or at the base of the mantle but farther southwest, in the African LLSVP [*Ritsema et al.*, 1999; *Courtillot et al.*, 2003]. In their recent study, *French and Romanowicz* [2015] show that the Afar plume is continuous down to the base of the upper mantle. The deep low-velocity anomaly that we observe beneath the Afar hot spots (see Figure 1) supports a connection down to the CMB through a rather vertical conduit that cannot be continuously mapped by the limited resolution of SEISGLOB1.

In order to visualize the new information present in SEISGLOB1 we display in Figure 2 the long-wavelength components of SEISGLOB1, SP12RTS, S362WMANI+M and SEMUCB-WM1 plotted up to the degree 8 as well as their even and odd parts. Figure 2 confirms that at 2700 km depth SEISGLOB1 agrees very well with the other models while at 2800 km depth SEISGLOB1 displays even and odd parts different from previous studies:

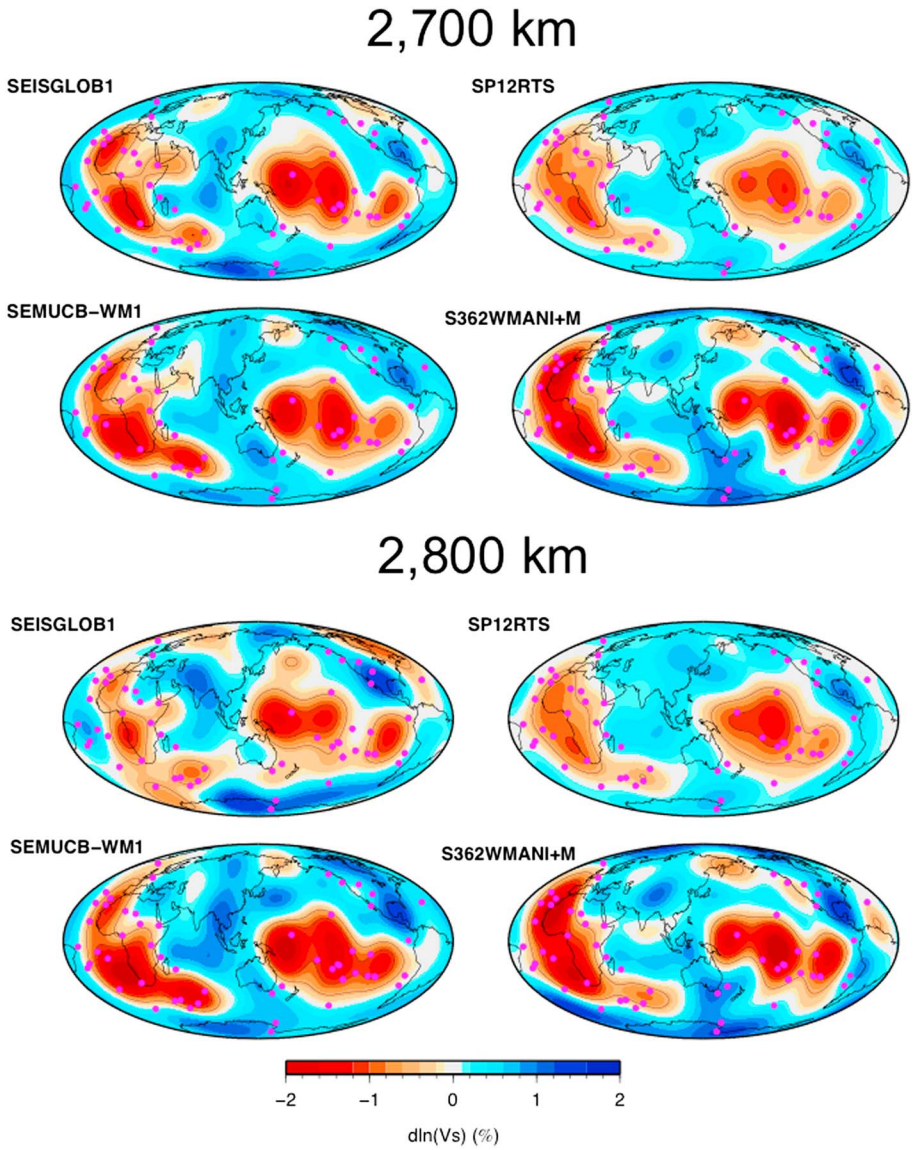

Figure 1. Shear velocity heterogeneities in SEISGLOB1 and other recent tomographic models (SEMUCB-WM1 [*French and Romanowicz*, 2014], S362WMANI+M [*Moulik and Ekström*, 2014], SP12RTS [*Koelemeijer et al.*, 2016]) filtered up to the degree 8 at 2700 and 2800 km depth. We also plot the contour lines at −0.50% and −1%. The color scale is in percent with respect to model PREM [*Dziewonski and Anderson*, 1981]. We can observe on SEISGLOB1 at 2800 km depth a possible deep mantle source for the Afar hot spot.

the even part has a weak amplitude similar to that observed in SP12RTS, the odd part is as strong as the even part. The complexity of the structure of the LLSVPs comes largely from the odd part. The individualization of the different regions in the African and Pacific LLSVPs corresponds to various low-velocity regions that are observed in the odd part which is constrained by new cross-coupling normal mode data.

Figure 2 thus confirms that SEISGLOB1 has different structure at the base of the mantle compared with the other models with a larger odd-even degree amplitude ratio and a change of the odd and even patterns. We have checked that by inverting only low-branch normal mode self-coupling data as in S40RTS we retrieve the well-known strong degree 2 at the base of the mantle (see Figure S2 in the supporting information). It is thus the addition of higher-branch self-coupling and Stoneley modes that imposes a decrease of the even degrees, a conclusion shared by SEISGLOB1 and SP12RTS. In addition, the inversion of cross-coupling normal modes in SEISGLOB1 requires a significant power in the odd degrees.

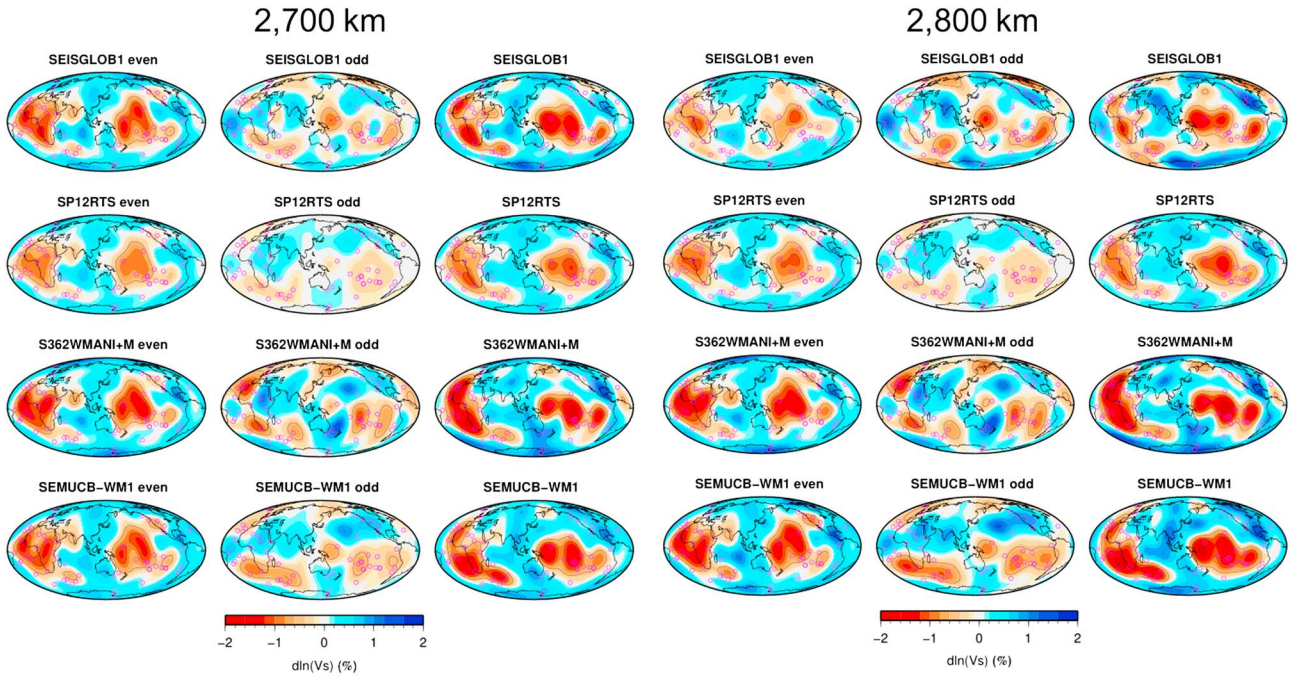

Figure 2. Maps of shear wave heterogeneities displayed at (left) 2700 km and (right) 2800 km for SEISGLOB1 and three other recent tomographic models [*Moulik and Ekström*, 2014; *French and Romanowicz*, 2014; *Koelemeijer et al.*, 2016] filtered up to the spherical harmonic degree 8. For each depth, panels represent from left to right: the even part, the odd part, and the sum of the two. Are also represented the −0.5% and −1% contour lines. SEISGLOB1 displays different even and odd patterns compared to the others at 2800 km depth.

This is also shown in Figure 3 *w* spectrum of SEISGLOB1 and the other tomographic models at 2700 and 2800 km depths (Figures 3, top left and 3, bottom left). It is noteworthy that at 2800 km depth, the degree 2 in SEISGLOB1 and SP12RTS is ≈ 50% smaller than in other models. Degree 3 appears to be 10% greater than the amplitude of degree 2 in SEISGLOB1, while it is at least 30% smaller in other seismic models. The odd degrees 5 and 7 have also a relatively large amplitude compared to the even degrees 4, 6, and 8. We also show in Figure 3 (right), the amplitude spectrum of SEISGLOB1 versus depth with the associated a posteriori errors for degrees 2 and 3 (color-shaded areas). For readability we only display on Figure 3 the errors on the degrees 2 and 3. It reveals that the importance of the odd degrees increases with depth and that they become larger than degree 2 as we approach the CMB. Moreover, this conclusion still holds when taking into account the a posteriori errors (in this depth range, the uncertainties for the even degrees are ≈10%, those for the odd degrees ≈20% except for degree 1, which is very poorly resolved with an uncertainty of ≈80%).

In Figure S3 we present the same plots as in Figure 3 but obtained with other (α, β) and (ρ, β) scaling laws (Figures S3, middle column and S3, left column). These tests show that whatever the scaling, a weaker degree 2 and stronger odd degrees are observed. In all cases the degree 3 becomes as large as degree 2 at some depth. However, a decrease of degree 2 across the D'' layer is only observed for a constant scaling law.

The amplitude of the degree 2 at the base of the mantle obtained from an inversion of body waves (SEMUCB-WM1) or body waves and low-order normal modes (S362WMANI+M) is significantly larger than when higher-branch self-coupling and Stoneley modes are included alone (SEISGLOB1) or in addition to body waves (SP12RTS) (see Figures 2 and S4). The very low degree 2 power in SEISGLOB1 is partly due to our choice of (α, β) and (ρ, β) scaling laws, and we do recover the degree 2 amplitude of SP12RTS when we use their scaling (see Figure S4), but this amplitude remains small compared to most previous models. It seems therefore that a degree 2 power as large as what is suggested by body wave analysis is not required by up to date normal modes, including higher-branch self-coupling normal modes and Stoneley modes. We speculate that this may be due to the uneven sampling of the lower mantle by body waves or to the difficulty in correcting for deep mantle anisotropy.

The quality of a tomographic model is of course revealed by its ability to provide a good fit to the data. We first checked that our numerical code is perfectly working by reproducing the same data as in Figure 9 of

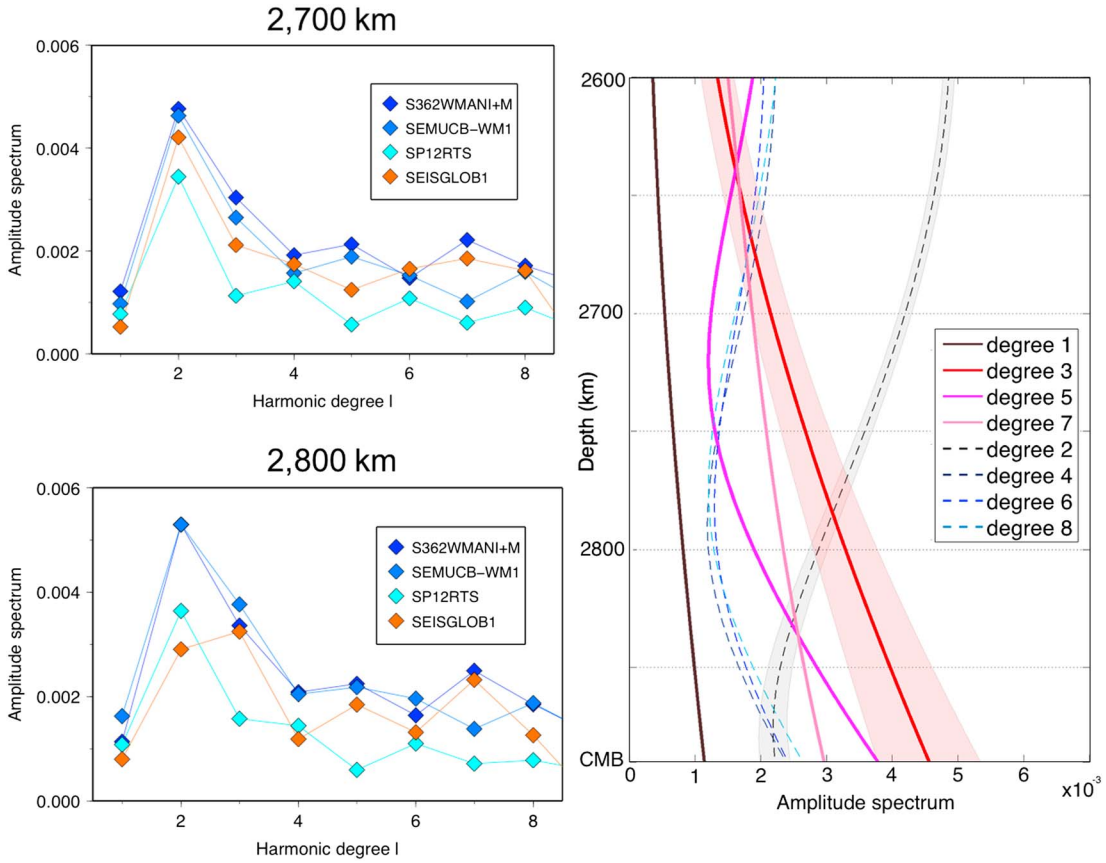

Figure 3. (left) Amplitude spectra of SEISGLOB1 and other tomographic models [*French and Romanowicz*, 2014; *Moulik and Ekström*, 2014; *Koelemeijer et al.*, 2016] at (top) 2700 and (bottom) 2800 km depth. (right) Amplitude spectrum and associated errors for degrees 2 and 3 (color-shaded areas) of SEISGLOB1 with depth from 2600 km depth down to the CMB. Even when considering the errors, our results still hold. Similar plots using other (α, β) and (ρ, β) scaling laws are depicted in Figure S3 in the supporting information.

Deuss et al. [2013], where they display some of their observations and the predictions obtained using S20RTS [*Ritsema et al.*, 2004] for some cross-coupling data. Figure S5 shows that, for these observations and this tomographic model, we are in perfect agreement with *Deuss et al.* [2013]. In Figure 4 we show how SEISGLOB1 and other models fit a few normal mode cross-coupling (rows 1–4), high-branch self-coupling (rows 5 and 6) and Stoneley mode self-coupling (rows 7 and 8) observations. Except for the top row, we choose observations that are particularly sensitive to the base of the mantle as seen by their sensibility kernels (Figure 4, column 1). We also provide at the bottom of Figure 4, a table that summarizes the misfits of the different models with the observations. Figure 4 shows that the cross-coupling observations are much better predicted by SEISGLOB1 than by all the previous models. Although this was expected (as these observations are only included in the inversion procedure of SEISGLOB1), this suggests that SEISGLOB1 takes into account an information on the long-wavelength structure which is not included in other models. For example, the pattern for ${}_9S_6 - {}_7S_9$, Figure 4 (row 2), is correctly predicted by the previous models but with a much too large amplitude while the pattern for ${}_{15}S_{16} - {}_{17}S_{15}$, Figure 4 (row 4), is poorly predicted by the previous models. It is usually for modes with sensibility kernels maximum near the CMB, such as for ${}_{15}S_{16} - {}_{17}S_{15}$, that SEISGLOB1 and the previous models significantly differ. The last two rows and the table in Figure 4 show that SEISGLOB1 also better explains Stoneley modes. In Table S4 we show the obtained misfit for the same modes but with the other tested scaling laws. The misfits are quite similar whatever is the scaling law except for the Stoneley mode ${}_1S_{13}$, where our parameterization gives a significantly better fit. Table S5 includes a few more quantitative assessments of the quality of SEISGLOB1, the results of the tests done with other scaling laws, and comparisons with other models.

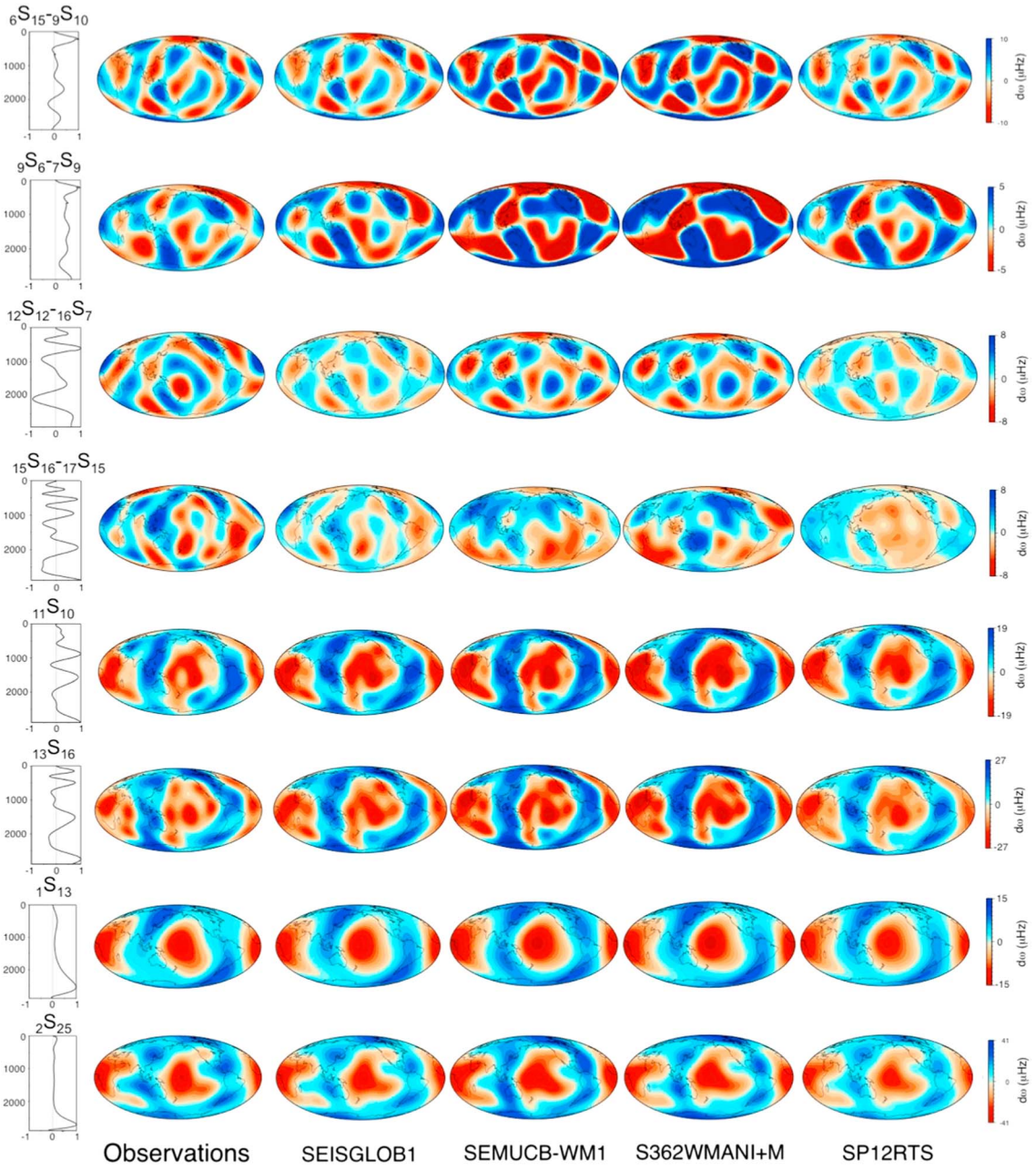

Models	$_6S_{15}$-$_9S_{10}$	$_9S_6$-$_7S_9$	$_{12}S_{12}$-$_{16}S_7$	$_{15}S_{16}$-$_{17}S_{15}$	$_{11}S_{10}$	$_{13}S_{16}$	$_1S_{13}$	$_2S_{25}$
SEISGLOB1	0.18	0.64	0.82	0.64	0.37	0.33	0.14	0.19
SEMUCB-WM1	0.87	2.00	1.10	1.09	0.61	0.52	0.26	0.38
S362WMANI+M	0.96	2.52	1.18	1.22	0.63	0.52	0.27	0.38
SP12RTS	0.41	0.82	0.74	1.01	0.38	0.34	0.25	0.26

Figure 4. (top, column 2) Observed and (columns 3–6) predicted splitting functions for the cross-coupling of the following modes: from top to bottom, (row 1) $_6S_{15}-_9S_{10}$, (row 2) $_9S_6-_7S_9$, (row 3) $_{12}S_{12}-_{16}S_7$, (row 4) $_{15}S_{16}-_{17}S_{15}$, (row 5) the self-coupling of some high-branch modes $_{11}S_{10}$ and (row 6) $_{13}S_{16}$, and the self-coupling of some Stoneley modes (row 7) $_1S_{13}$ and (row 8) $_2S_{25}$. The observations have been computed from the measurements of *Deuss et al.* [2013] for the self- and cross-coupling data and from the measurements of *Koelemeijer et al.* [2013] for the Stoneley modes. (column 1) The corresponding normalized shear velocity kernels from the surface down to the CMB. Some of these normal mode data are particularly sensitive to the velocity structure close to the CMB ($_{12}S_{12}-_{16}S_7$, $_{15}S_{16}-_{17}S_{15}$, $_{11}S_{10}$, $_{13}S_{16}$, $_1S_{13}$, and $_2S_{15}$), and in that case SEISGLOB1 better explains the observations. This is illustrated in the table below. (bottom) Table of the misfit for each considered mode self- and cross-coupling. The misfit is defined for a given data *i* as $M_i = \sqrt{\sum_{st}\left[\left(c^t_{s,synth} - c^t_{s,obs}\right)^2\right] / \sum_{st}\left[\left(c^t_{s,obs}\right)^2\right]}$ where *s* and *t* are, respectively, the spherical harmonic degrees and orders, $c^t_{s,obs}$ are the measured self- and cross-coupling coefficients and $c^t_{s,synth}$ the self- or cross-coupling coefficients computed in various tomographic models.

4. Implications

SEISGLOB1 allows us to refine the broad-scale structure at the bottom of the mantle. We show that this new large-scale pattern is related to a larger odd-even degree amplitude ratio at the base of the mantle. Differently from previous findings, the large rather homogeneous LLSVPs found in previous model seem composed of individual maxima often located beneath hot spots. This new pattern is likely related to the history of mantle convection so that geodynamicists will have to investigate how to generate such a pattern. It has already been shown in numerical models that the degree 2 tends to stabilize the LLSVPs [*Forte et al.*, 2002], but does it still hold with weaker even degrees? Finally, several evidences from laboratory experiments [*Forte et al.*, 2002] and numerical modeling [*Bloxham*, 2000; *Amit et al.*, 2008; *Olson et al.*, 2010; *Gubbins et al.*, 2011; *Driscoll*, 2015] support the influence of the deepest mantle on the outer core fluid flow and thus on the topology of the geodynamo. For instance, *Driscoll* [2015] shows that applying a CMB heat flux that contains only degree and mode 2 generates a similar structure on the inner core boundary but shifted at 30° westward. It has also been shown that the heterogeneous CMB heat flux controlled by the lower mantle heterogeneities can significantly affect the geomagnetic reversal frequency [*Olson et al.*, 2010] and its secular variations [*Bloxham*, 2000]. Since the recent tomographic models were dominated by the spherical harmonic degree 2 at the base of the mantle (see Figure 3), the applied heat flux pattern in these studies was dominated by the degree 2. However, the thermal control from the lower mantle can drastically affect the fluid flow in the outer core, and changing this forcing may greatly influence the predictions. For instance, the existence of weaker even degrees and a stronger contribution of odd degrees could help in understanding how the hemispherical [*Tanaka and Hamaguchi*, 1997; *Niu and Wen*, 2001] structure of the inner core has appeared. It is thus of crucial importance to continue to measure the normal mode self- and cross-coupling which will enable us to refine the large-scale lowermost mantle structure.

5. Concluding Remarks

We have presented SEISGLOB1, a pure SV model of Earth's mantle. The simultaneous inversion of new normal mode cross-coupling measurements that have never been included in any tomographic models, self-coupling of low- and high-order normal modes, including Stoneley modes and Rayleigh phase velocities, enables us to bring new constraints on the large-scale structure at the base of the mantle. We show that the velocity structure at the base of the mantle is more complex than that from a dominant degree 2 and that the odd degrees become relatively larger as one approaches the CMB. This new pattern can have strong implications on the heat flux imposed at the CMB which controls the outer dynamics and has to be taken into account in future outer core dynamic simulations.

Acknowledgments
This work was supported by the French ANR SEISGLOBANR-11-BLANC-SIMI5-6-016-01, the European Research Council within the framework of the SP2-Ideas Program ERC-2013-CoG, under ERC grant agreement 617588 and the German Deutsch Forschungsgemeinschaft under the DFG project HAADES DU 1634/1-1.

References

Amit, H., J. Aubert, G. Hulot, and P. Olson (2008), A simple model for mantle-driven flow at the top of Earth's core, *Earth Planets Space*, *60*, 845–854.

Benoit, M. H., A. A. Nyblade, T. J. Owens, and G. Stuart (2006), Mantle transition zone structure and upper mantle S velocity variarions beneath Ethiopia: Evidence for a broad, deep-seated thermal anomaly, *Geochem. Geophys. Geosyst.*, *7*, Q11013, doi:10.1029/2006GC001398.

Bloxham, J. (2000), The effect of thermal core-mantle interactions on the paleomagnetic secular variations, *Philos. Trans. R. Soc. A*, *358*, 1171–1179.

Bullen, K. E. (1949), Compressibility-pressure hypothesis and the Earth's interior, *Geophys. J. Int.*, *5*, 355–368.

Chang, S-J., and S. Van der Lee (2011), Mantle plumes and associated flow beneath Arabia and East Africa, *Earth Planet. Sci. Lett.*, *301*, 448–454.

Chang, S-J., A. M. G. Ferreira, J. Ritsema, H. J. van Heijst, and J. H. Woodhouse (2015), Joint inversion for global isotropic and radially anisotropic mantle structure including crustal thickness perturbations, *J. Geophys. Res. Solid Earth*, *120*, 4278–4300, doi:10.1002/2014JB011824.

Courtillot, V., A. Davaille, J. Besse, and J. Stock (2003), Three distinct types of hotspots in the Earth's mantle, *Earth Planet. Sci. Lett.*, *205*, 295–308.

Debayle, E., J. J. Lévêque, and M. Cara (2001), Seismic evidence for a deeply rooted low velocity anomaly in the upper mantle beneath the northeastern Afro/Arabian continent, *Earth Planet. Sci. Lett.*, *193*(3–4), 369–382.

Debayle, E., and M. Sambridge (2004), Inversion of massive surface wave data sets: Model construction and resolution assessments, *J. Geophys. Res.*, *109*, B02316, doi:10.1029/2003JB002652.

Debayle, E., and Y. Ricard (2012), A global shear velocity model of the upper mantle from fundamental and higher Rayleigh mode measurements, *J. Geophys. Res.*, *117*, B10308, doi:10.1029/2012JB009288.

Deuss, A., J. Ritsema, and H. van Heijst (2013), A new catalog of normal-mode splitting function measurements up to 10 mHz, *Geophys. J. Int.*, *193*, 920–937.

Driscoll, P. (2015), Testing the dynamic coupling of the core-mantle and inner core boundaries, *J. Geophys. Res. Solid Earth*, *120*, 4689–4701, doi:10.1002/2014JB011682.

Durand, S., E. Debayle, and Y. Ricard (2015), Rayleigh wave phase velocity and error maps up to the fifth overtone, *Geophys. Res. Lett.*, *42*, 3266–3272, doi:10.1002/2015GL063700.
Dziewonski, A., B. Hager, and R. O'Connell (1977), Large-scale heterogeneities in the lower mantle, *J. Geophys. Res.*, *82*, 239–255.
Dziewonski, A. M., and D. l. Anderson (1981), Preliminary reference Earth model, *Phys. Earth Planet. Inter.*, *25*, 297–236.
Ford, S., E. J. Garnero, and A. K. McNamara (2006), A strong lateral shear velocity gradient and anisotropy heterogeneity in the lowermost mantle beneath the southern Pacific, *J. Geophys. Res.*, *111*, B03306, doi:10.1029/2004JB003574.
Forte, A., J. Mitrovica, and A. Espesset (2002), Geodynamic and seismic constraints on the thermochemical structure and dynamics of convection in the deep mantle, *Philos. Trans. R. Soc. A*, *360*(1800), 2521–2543.
French, S. W., and B. Romanowicz (2014), Whole-mantle radially anisotropic shear-velocity structure from spectral-element waveform tomography, *Geophys. J. Int.*, *199*, 1303–1327.
French, S. W., and B. Romanowicz (2015), Broad plumes rooted at the base of the Earth's mantle beneath major hotspots, *Nature*, *525*, 95–97.
Gubbins, D., B. Sreenivasan, J. Mound, and S. Rost (2011), Melting of the Earth's inner core, *Nature*, *473*, 361–364.
Ishii, M., and J. Tromp (2001), Even-degree lateral variations in the mantle constrained by free oscillations and the free-air gravity anomaly, *Geophys. J. Int.*, *145*, 77–96.
Kendall, J.-M., and P. G. Silver (1996), Constraints from seismic anisotropy on the nature of the lowermost mantle, *Nature*, *381*, 409–412.
Koelemeijer, P. J., A. Deuss, and J. Ritsema (2013), Observations of core-mantle boundary Stoneley modes, *Geophys. Res. Lett.*, *40*, 2557–2561, doi:10.1002/grl.50514.
Koelemeijer, P. J., J. Ritsema, A. Deuss, and H-J. van Heijst (2016), SP12RTS: A degree-12 model of shear- and compressional-wave velocity for Earth's mantle, *Geophys. J. Int.*, *204*, 1024–1039.
Lekic, V., S. Cottaar, A. Dziewonski, and B. Romanowicz (2012), Cluster analysis of global lower mantle tomography: A new class of structure and implications for chemical heterogeneity, *Earth Planet. Sci. Lett.*, *357–358*, 68–77.
Masters, G., G. Laske, and F. Gilbert (2000), Matrix auto-regressive analysis of free oscillation coupling and splitting, *J. Geophys. Res.*, *143*, 478–489.
Montagner, J. (1986), Regional three-dimensional structures using long period surface waves, *Ann. Geophys.*, *4*, 283–294.
Moulik, P., and G. Ekström (2014), An anisotropic shear velocity model of the Earth's mantle using normal modes, body waves, surface waves and long-period waveforms, *Geophys. J. Int.*, *199*(3), 1713–1738.
Niu, F. L., and L. X. Wen (2001), Hemispherical variations in seismic velocity at the top of the Earth's inner core, *Nature*, *410*, 1081–1084.
Olson, P., S. C. Robert, P. Driscoll, G. G latzmaier, and P. Roberts (2010), Geodynamo reversal frequency and heterogeneous core-mantle boundary heat flow, *Phys. Earth Planet. Inter.*, *180*, 66–79.
Resovsky, J. S., and M. H. Ritzwoller (1998), New and refined constraints on 3-D Earth structure from normal modes below 3 mHz, *J. Geophys. Res.*, *103*, 783–810.
Resovsky, J. S., and M. H. Ritzwoller (1999), A degree 8 mantle shear velocity model from normal mode observations below 3 mHz, *J. Geophys. Res.*, *104*, 993–1014.
Ricard, Y., M. Richards, C. Lithgow-Bertelloni, and Y. Le Stunff (1993), A geodynamic model of mantle density heterogeneities, *J. Geophys. Res.*, *98*, 21,895–21,909.
Ritsema, J. (2000), Evidence for shear velocity anisotropy in the lowermost mantle beneath the Indian Ocean, *Geophys. Res. Lett.*, *27*, 1041–1044.
Ritsema, J., H. J. ven Heijst, and J. H. Woodhouse (1999), Complex shear wave velocity structure imaged beneath Africa and Iceland, *Science*, *286*, 1925–1928.
Ritsema, J., H. van Heijst, and J. H. Woodhouse (2004), Global transition zone tomography, *J. Geophys. Res.*, *109*, B02302, doi:10.1029/2003JB002610.
Ritsema, J., A. Deuss, H. J. van Heijst, and J. H. Woodhouse (2011), S40RTS: A degree-40 shear-velocity model for the mantle from new Rayleigh wave dispersion, teleseismic traveltime and normal-mode splitting function measurements, *Geophys. J. Int.*, *184*, 1223–1236.
Smith, M. F., and G. Masters (1989), Aspherical structure constraints from free oscillation frequency and attenuation measurements, *J. Geophys. Res.*, *94*, 1953–1976.
Tanaka, S., and H. Hamaguchi (1997), Degree one heterogeneity and hemispherical variation of anisotropy in the inner core from PKP(BC)-PKP(DF) times, *J. Geophys. Res.*, *102*, 2925–2938.
Tarantola, A., and B. Valette (1982), Generalized nonlinear inverse problems solved using the least square criterion, *Rev. Geophys.*, *20*, 219–232.
Woodhouse, J. H. (1980), The coupling and attenuation of nearly resonant multiplets in the Earth's free oscillation spectrum, *Geophys. J. R. Astron. Soc.*, *61*, 261–283.
Woodhouse, J. H., D. Giardini, and X. D. Li (1986), Evidence for inner core anisotropy from free oscillations, *Geophys. Res. Lett.*, *13*, 1549–1552.